Supplemental Material: Conductivity in the square lattice Hubbard model at high temperatures: importance of vertex corrections

J. Vučičević,[1] J. Kokalj,[2,3] R. Žitko,[3,4] N. Wentzell,[5] D. Tanasković,[1] and J. Mravlje[3]

[1] *Scientific Computing Laboratory, Center for the Study of Complex Systems, Institute of Physics Belgrade, University of Belgrade, Pregrevica 118, 11080 Belgrade, Serbia*

[2] *University of Ljubljana, Faculty of Civil and Geodetic Engineering, Jamova 2, Ljubljana, Slovenia*

[3] *Jozef Stefan Institute, Jamova 39, SI-1000, Ljubljana, Slovenia*

[4] *University of Ljubljana, Faculty of Mathematics and Physics, Jadranska 19, Ljubljana, Slovenia*

[5] *Center for Computational Quantum Physics, Simons Foundation Flatiron Institute, New York, NY 10010 USA*

Here we present a detailed analysis of the numerical results that we perform to disentangle the different contributions to the optical conductivity and identify the source of discrepancy between DMFT and FTLM. The analysis is performed on the imaginary axis where we can obtain the results from CTINT. Note that at high temperature, the Matsubara frequencies are far apart and the values of $\Lambda(i\nu_n)$ are insensitive to the details of $\sigma(\omega)$. We illustrate this in Fig. S1 where we show that, on the Matsubara axis, the FTLM and DMFT $\Lambda(i\nu_n)$ results are almost indistinguishable. However, the discrepancy is *not* below the level of noise in our numerics and we are able to reconstruct this difference from three different contributions, namely the finite-size effects, non-local self-energy effects and vertex corrections, all obtained independently using combinations of other methods. However, in the present context, we find the CTINT method useful only as a tool for benchmarking, since the analytical continuation from the imaginary to the real axis introduces a systematic error, and a precise σ_{dc} value is difficult to extract from $\Lambda(i\nu_n)$. In Section I we present our imaginary axis analysis of the results, and in Section II we discuss the difficulty of analytical continuation. Then, in Section III we benchmark our FTLM result against analytically computed frequency moments of the optical conductivity. In Section IV we discuss the details of the pole-broadening procedure used in FTLM.

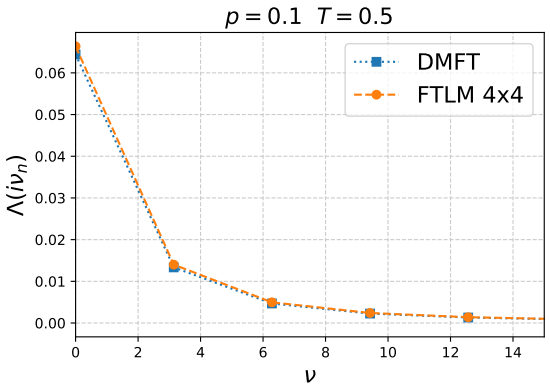

FIG. S1. Current-current correlation function $\Lambda(i\nu_n)$ in FTLM and DMFT (the dashed and dotted lines are guides to the eye).

I. DETAILED BENCHMARK

In Fig. S2 we show the detailed comparison and cross-checks between the different methods in 12 doping-temperature (p, T) points in the Hubbard model phase diagram at $U = 2.5D = 10t$. The continuous lines are obtained by the Hilbert transform from the real-axis to the continuous imaginary variable $\sigma(\omega) \to \Lambda(i\nu)$, and then taking the difference between the different methods, as written in the legend. The question we are addressing in the main text and that is considered in further detail here is the physical origin of the difference difference between DMFT and FTLM 4×4, presented on Fig. S2 by the orange lines.

We can readily inspect the effect of finite cluster size on the bubble Λ^{disc}. This is given by the red line which presents the difference between DMFT 4×4 and DMFT. Red circles are obtained independently on the Matsubara axis without any analytical continuation, directly from DMFT data (DMFT here is performed with CTINT solver), and present an additional cross-check of our analytical continuation of the self-energy which was used to obtain $\sigma(\omega)$ in DMFT. We note that the statistical noise coming from CTINT in the single-site DMFT solution is very small, and the Padé analytical continuation of $\Sigma(i\omega_n)$ can be successfully performed. The optical conductivities agree closely (within few percent) between QMC and the numerical renormalization group (NRG) solution.

We can also compare the red line with the difference between the full Λ from CTINT 8×8 and 4×4 (purple crosses). The agreement is solid: it appears that the only difference between the 8×8 and 4×4 clusters is the finite-size effects in the bubble Λ^{disc}, and that the finite-size effects disappear entirely already at cluster size 8×8. Note, however, that finite-size effects mostly pertain to the overall integral of $\sigma(\omega)$ (i.e. $\Lambda(i\nu = 0)$),

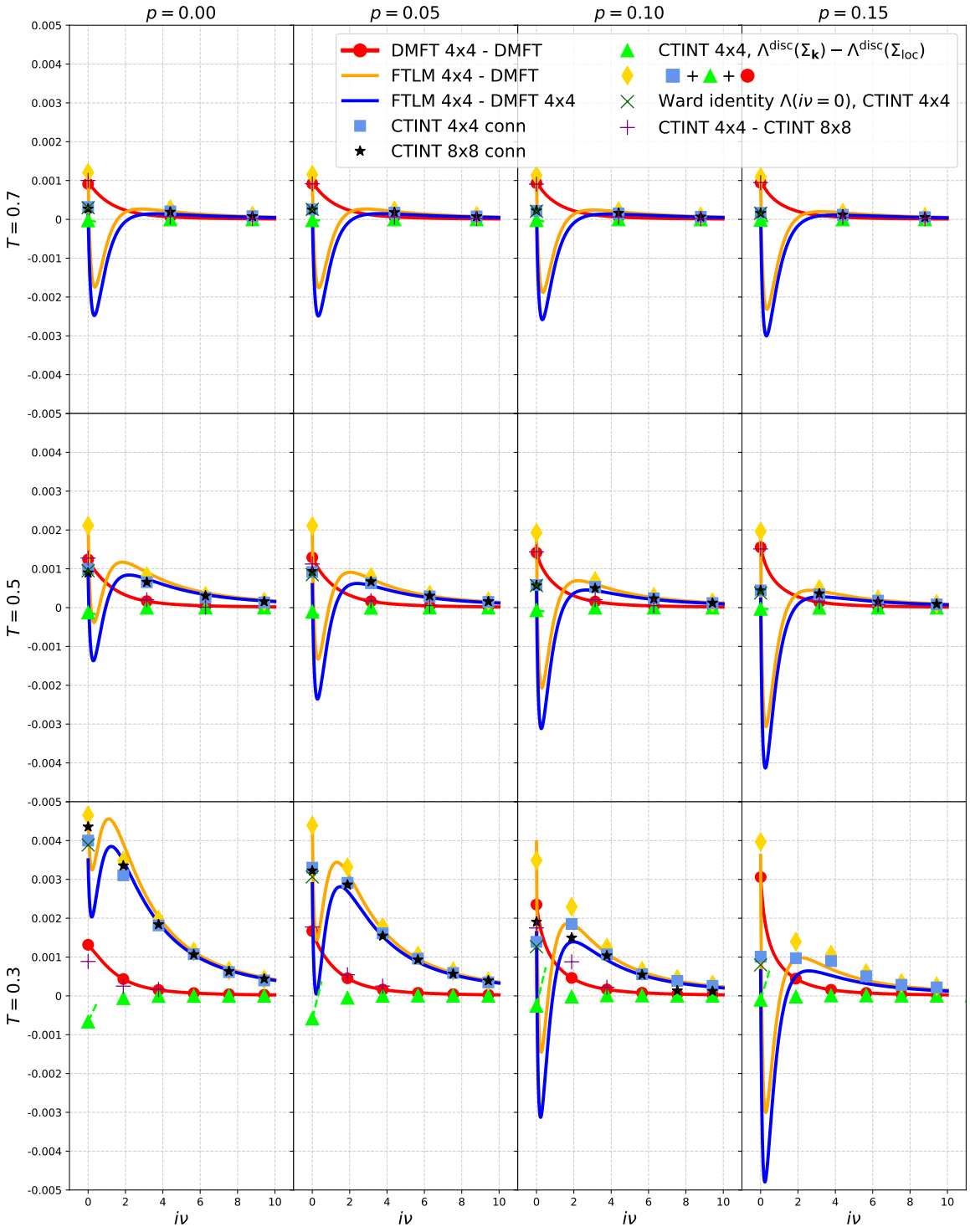

FIG. S2. Comparison of various parts of the current-current correlation functions $\Lambda(i\nu)$ on the imaginary axis (see text).

and have little impact on $\sigma_{\rm dc}$.

The blue line presents the difference between FTLM 4×4 and DMFT 4×4, which is by construction the orange line minus the red line, i.e. the difference between DMFT and FTLM 4×4, up to the finite-size effects in the bubble.

The blue squares and black stars are the vertex corrections $\Lambda^{\rm conn}$ as obtained from CTINT 4×4 and 8×8: at $T\geq0.5D$ their agreement is excellent, and even at the lowest temperature it is likely within the statistical error bars of the method. At the lowest temperature there is some discrepancy but mostly due to increased statistical error in CTINT. The problem particularly pronounced at the biggest doping, where our CTINT 8×8 calculation suffers from the sign problem and failed to converge properly in the available computational time (384 `cpu*days` per point).

We have inspected also the self-energies and found excellent agreement between CTINT 8×8 and 4×4 (see Fig.3a in main text, other data not shown). We observe that the range of $\Sigma_{\mathbf{r}}$ is at most 2 lattice spacings, which means that the longer distance components that are captured by the 8×8 cluster are unlikely to have a measurable effect on any observable.

We cross check our results by calculating $\Lambda^{\rm conn}(i\nu=0)$ from the Ward identity[1].

$$\Lambda^{\rm conn}(i\nu=0)=-2T\sum_{\mathbf{k}}v_{\mathbf{k}}\sum_{i\omega_n}G^2_{\mathbf{k}}(i\omega_n)\partial_{k_x}\Sigma_{\mathbf{k}}(i\omega_n)$$

and present it using the dark-green cross. Here we have constructed $\Sigma_{\mathbf{k}}(i\omega_n)$ on the lattice (64×64 grid Brillouin zone) using the Fourier transform of the short-distance $\Sigma_{\mathbf{r}}$ components available on the 4×4 cluster, which also allowed us to take the derivative analytically. Again, the agreement with the corresponding blue square and black star is within the roughly estimated statistical error of CTINT at all temperatures.

In most cases the blue line (difference between FTLM 4×4 and DMFT 4×4) passes through the blue squares (vertex correction from CTINT 4×4). However, at $i\nu=0$ there appears to be a systematic deviation, and the blue line passes below the blue square. This we can link to the effect of non-local self-energy on the bubble which we calculate from the CTINT 4×4 results and present as green color triangles. Indeed, the green triangles are mostly negligible except at $\nu=0$ where they are slightly negative.

We check our decomposition by summing the green triangles, blue squares and red circles, and comparing them to the orange line. Within statistical error bars, the total difference between FTLM4×4 and DMFT appears to come from 1) finite-size effects in the bubble, 2) effects of non-local self-energy in the bubble and 3) vertex corrections.

Note, however, that the effects of non-local self-energy on the bubble are small and visible only at the lowest temperature, and related only to the overall integral of $\sigma(\omega)$, i.e. the kinetic energy. The only measurable effect on $\sigma(\omega=0)=-\partial_\nu\Lambda(i\nu)|_{\nu\to0^+}$ appears to come from the vertex corrections. We additionally cross check this by analytically continuing $\Sigma_{\mathbf{r}\neq0}$ from CTINT 4×4 and using it together with DMFT $\Sigma_{\rm loc}(\omega)$ that we already have on the real-axis from NRG solver, to construct $\Sigma_{\mathbf{k}}(\omega)$ and calculate $\sigma^{\rm disc}(\omega=0)$. The difference from the pure DMFT result is negligible in relative terms except at $p=0$ and lowest T where $\sigma_{\rm dc}$ becomes very small. We present the corresponding slope in $\Lambda(i\nu)$ with green color dashed lines and see that it is much smaller that the slope of the blue line, and even in the opposite direction.

Based on the above analysis we conclude that at $T\gtrsim0.3D$, finite-size effects and the effect of non-local self-energy on $\sigma^{\rm disc}_{\rm dc}$ become negligible, and that the vertex corrections $\sigma^{\rm conn}_{\rm dc}$ are already well converged with respect to the cluster size at the size 4×4. This builds confidence that our FTLM 4×4 is close to exact solution of the bulk Hubbard model.

II. UNCERTAINTIES IN THE ANALYTICAL CONTINUATION OF $\Lambda(i\nu_n)$

In this section we thoroughly test the Maximum Entropy analytical continuation (MaxEnt) of the Matsubara current-current correlation function $\Lambda(i\nu_n)\to\sigma(\omega)$. We find that the result is strongly biased towards the model function used in MaxEnt continuation, and therefore discard the CTINT results for $\sigma(\omega)$ in favor of FTLM 4×4 which requires no analytical continuation.

In Fig. S3 we compare $\sigma(\omega)$ and $\Lambda(i\nu)$ between FTLM and DMFT. As a function of continuous imaginary variable, $\Lambda(i\nu)$ is displayed by a line, and the Matsubara frequencies are indicated with crosses. Note that only the values at the Matsubara frequencies $\Lambda(i\nu_n)$ serve as the input for MaxEnt. We see that most of the difference between FTLM and DMFT is encoded between the first two Matsubara frequencies in $\Lambda(i\nu)$. In particular, the dc conductivity is given by $\sigma_{\rm dc}=-\partial_\nu\Lambda(i\nu)|_{\nu\to0^+}$, which is hard to estimate based on $\Lambda(i\nu_n)$. Although there is a one-to-one correspondence between any given function on the real axis and its Hilbert transform on the imaginary axis, any amount of noise in $\Lambda(i\nu_n)$ and a truncation of Matsubara frequencies is likely to lead to loss of critical information necessary to distinguish between two similar $\sigma(\omega)$.

Fig. S4 shows the optical conductivity obtained by the analytical continuation of the current-current correlation function $\Lambda(i\nu_n)$ from CTINT. We use the implementation of the Maximum Entropy method from

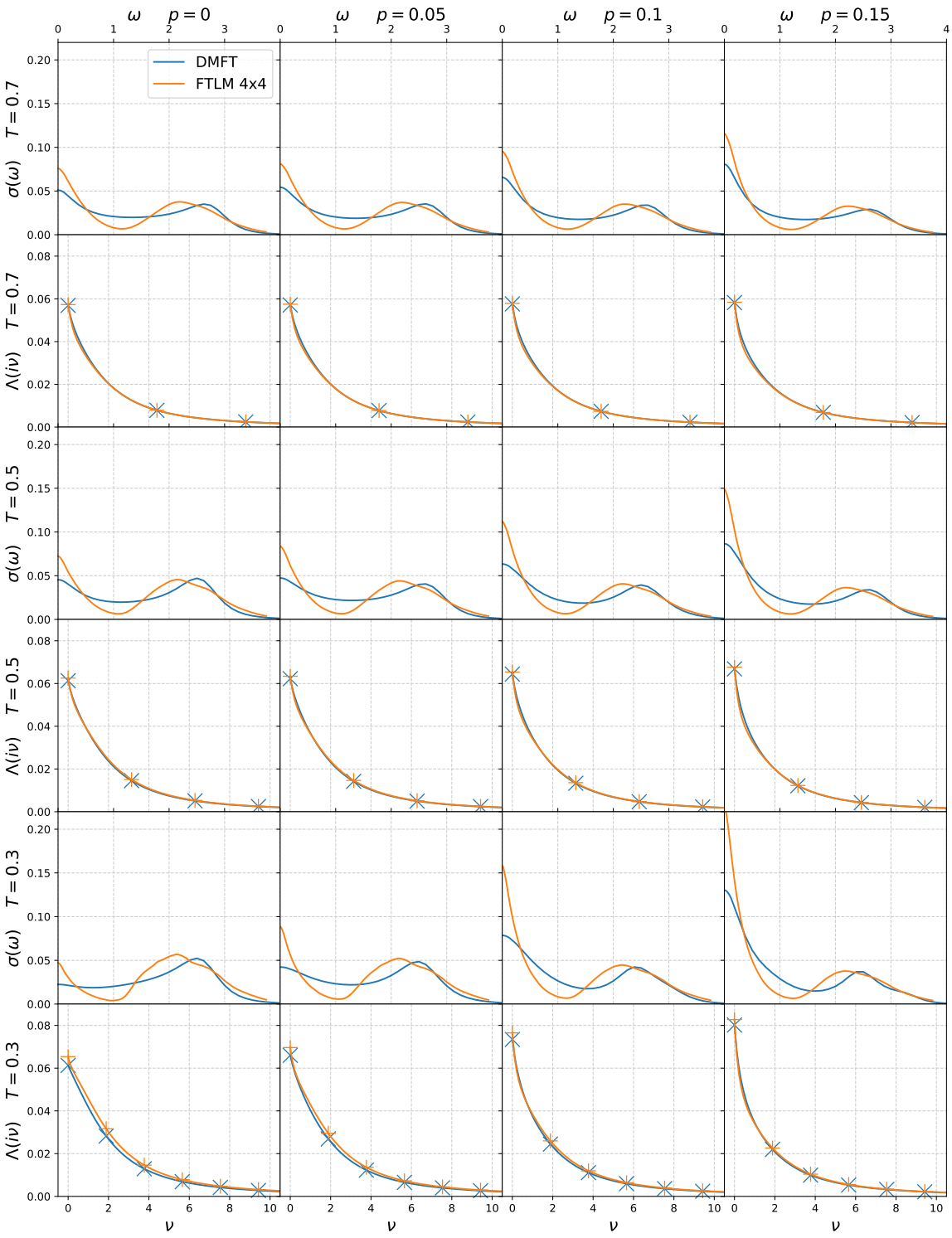

FIG. S3. Optical conductivity and current-current correlation function (see text).

Ref. 2. We put the error bar $d\Lambda(i\nu_n) = 10^{-4}$. Below this value the MaxEnt $\sigma(\omega)$ starts to acquire noisy and manifestly wrong features, due to overfitting. This value of 10^{-4} also agrees with the deviation in $\Lambda(i\nu_n)$ between CTINT 4×4 and FTLM, attributed to the statistical noise in CTINT. We perform annealing similar to Ref. 3: we apply MaxEnt at temperature $T = 0.5D$, using either FTLM (left column) or DMFT (middle column) $\sigma(\omega)$ at $T = 0.7$ as the default model. MaxEnt is then done at $T = 0.3D$, using the result of previous MaxEnt as the default model. The right column in Fig. S4 shows the resulting dc resistivities.

We see that the result of the analytical continuation strongly depends on the initial model function at high temperature. Furthermore, when the initial model is given by FTLM, the result at $T = 0.3$ still tends to deviate towards the DMFT solution. The reason for this is that the Drude-like peak in DMFT is broader than in FTLM, and the MaxEnt generally tends to make the spectrum smoother. This means that even with the correct default model at the highest temperature, the error bar introduced by annealing can easily erase any information about the vertex corrections and produce a result comparable to just the bubble contribution that one can safely obtain from DMFT(NRG). When the initial default model is taken to be DMFT, the error bar goes up to 50 percent, and the results typically resemble the DMFT solution.

Instead of choosing as the default model the FTLM results, which are computationally expensive to obtain (around one month on 32 cores with 80 GB of RAM for single choice of boundary conditions), it may appear reasonable to try and start the annealing using the high-T expansion[4] result at the highest temperature. However, as shown in Ref. 3 even high-T expansion is not trivial to calculate, and can only yield $\sigma(t)$ results up to $t \approx 1$ (t here is real time). In Fig. S5 we illustrate how the short time conductivity holds little information about $\sigma_{\rm dc}$ as $\sigma_{\rm dc} \sim \int dt {\rm Re}\sigma(t)$. The error made in the high-T expansion then propagates in MaxEnt, and can lead to wrong results.

Finally, it should be noted that with increasing temperature, Matsubara frequencies spread out, leaving less and less information to be extracted from even a slightly noisy $\Lambda(i\nu_n)$. We conclude that doing MaxEnt on CTINT 8×8 even with the corresponding FTLM 4×4 default model would not bring any information other than what is already contained in FTLM. Our analysis highlights the importance of developing methods that calculate the current-current correlation function directly on the real frequency axis.

III. COMPARISON WITH THE MOMENTS FROM THE HIGH-TEMPERATURE EXPANSION

In the high-T limit with $\sigma(\omega) \propto 1/T$, the frequency moments $\mu_k = \frac{1}{2\pi}\int_{-\infty}^{\infty}\sigma(\omega)\omega^k d\omega$ can be calculated reliably or even analytically[3,4] as the expectation values of certain commutators between the Hamiltonian and the current operator. Despite the difficult to reconstruct $\sigma(\omega)$, and in particular $\sigma_{\rm dc}$ from such moments with high confidence[3], the moments still provide a firm test of the numerical approaches.

By using the real frequency $\sigma(\omega)$ obtained with FTLM, we calculate frequency moments in the high-T limit for $U = 1.5D$ and $p = 0.2$. Such moments can be compared to the exact values reported in Ref. 3. We find that our FTLM moments μ_k for $k = 0 - 8$, which have main contributions from $\sigma(\omega)$ in the regime $|\omega| \lesssim 4D$ (i.e. up to ω about $2D$ above the upper edge of the Hubbard band), deviate from the exact moments by $\lesssim 0.2\%$. Some lower moments show even smaller deviation (see Table S1), which suggest FTLM correctly reproduces high-T behavior with small finite size effects. Our higher moments ($k \gtrsim 10$) show systematic larger deviation from the exact results due to high frequency cutoff at $\omega > 5D$ in our FTLM results.

$T \to \infty$ values of the FTLM moments are obtained by fitting T dependence of $2T\mu_k$ to $a + b/T^2$ in the temperature range between $5D$ and $10D$. The numerical uncertainties given in brackets in the Table S1 are obtained as a standard deviation in the fitting procedure.

k	$2T\mu_k$ (exact)	$2T\mu_k$ (FTLM)
0	0.96	0.96001(9)
2	16.5888	16.554(4)
4	879.206	879.4(2)
6	71350.4	71525(20)
8	$7.95719 \cdot 10^6$	$7.963(2) \cdot 10^6$

TABLE S1. Exact frequency moments $2T\mu_k$ taken from Ref. 3 and the moments from integrating FTLM $\sigma(\omega)$ (here the units of $t = D/4 = 1$ are used). The numbers in the brackets are estimates of numerical uncertainty for the last digits. Small deviations of FTLM moments from exact values suggest small finite size effects in the high-T limit.

IV. BROADENING IN FTLM

Optical conductivity calculated with FTLM on a finite cluster is strictly a set of delta functions in frequency space. The number of such delta functions grows with the number of many-body states, leading to a high density for the used cluster sizes. Still, the delta functions

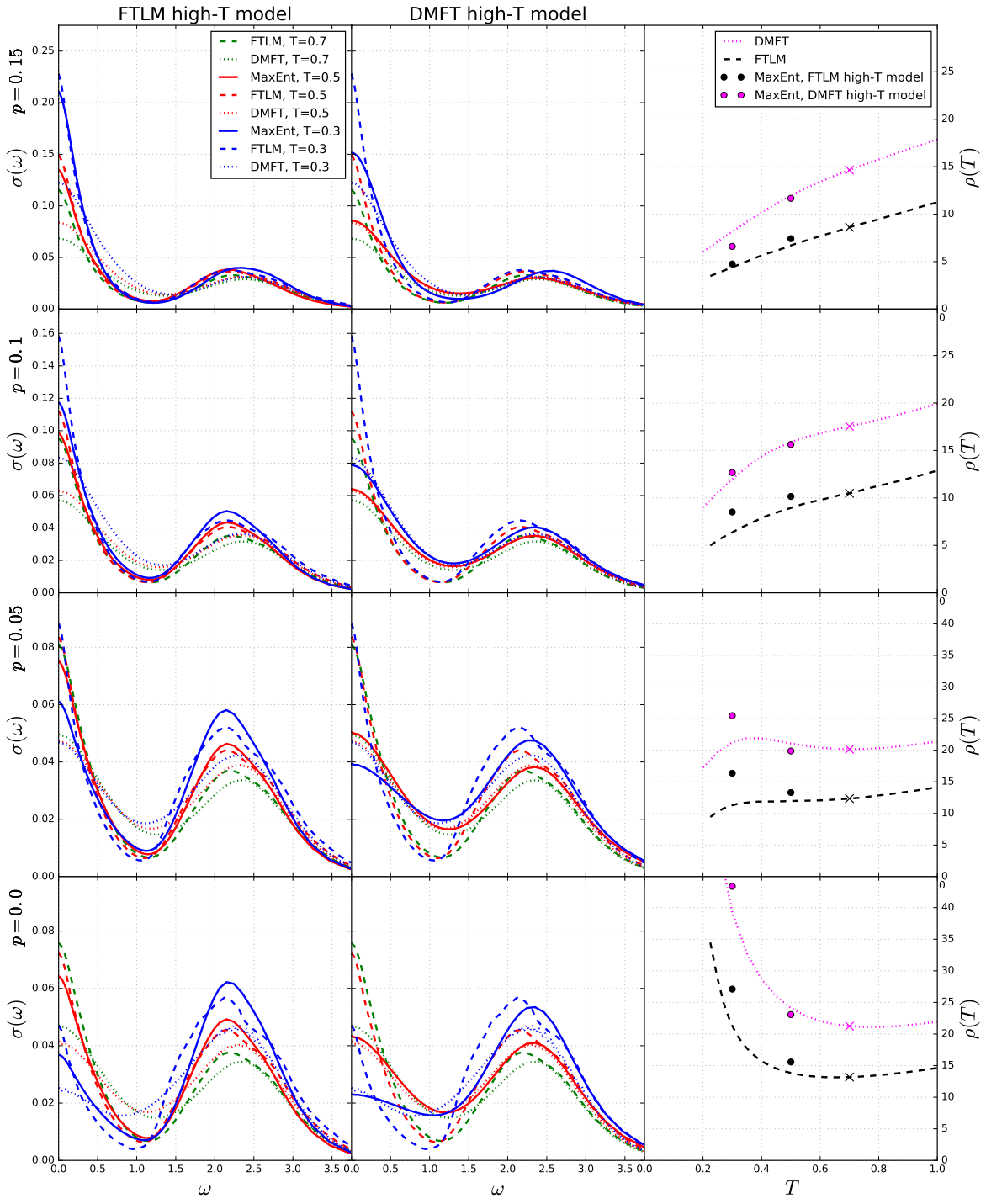

FIG. S4. Optical conductivity obtained by MaxEnt analytical continuation of the CTINT $\Lambda(i\nu_n)$ (solid lines in the first and the second column). The annealing method is used, where the initial model function, used for MaxEnt at $T = 0.5$, is the FTLM (first column), and DMFT (second column) at $T = 0.7$. At $T = 0.3$ the model function is the MaxEnt result from $T = 0.5$. The dashed (dotted) lines are FTLM (DMFT) data. The right column shows the MaxEnt resistivities, $\rho = 1/\sigma(\omega = 0)$, in comparison with FTLM and DMFT $\rho(T)$ curves. The four rows correspond to different doping levels $p = 0.15, 0.1, 0.05, 0$. The crosses are the dc resistivity corresponding to the initial model function.

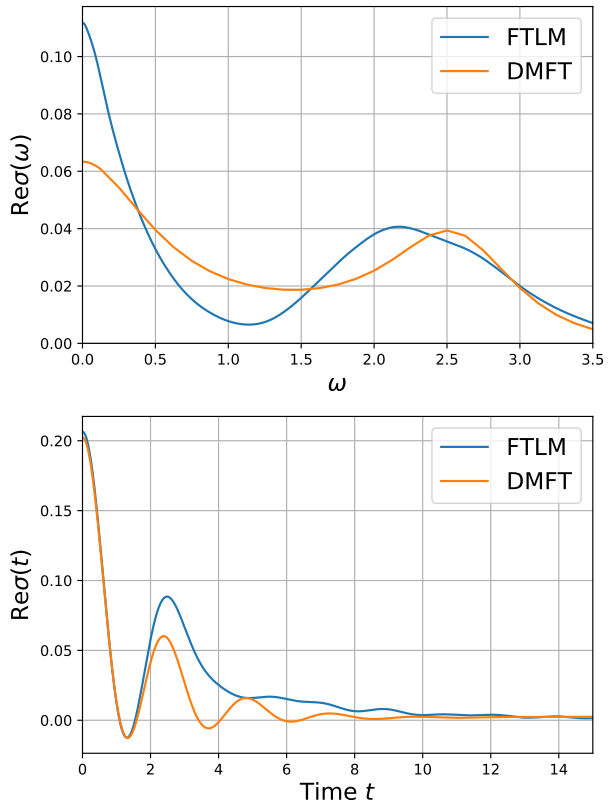

FIG. S5. Optical conductivity and its Fourier transform at $p = 0.1$, $T = 0.5D$. The dc conductivity has contributions from up to $t \sim 10$. DMFT and FTLM practically coincide at $t < 1$.

need to be broadened to get a smooth spectra, representative of the thermodynamic limit. The value of the broadening needs to be appropriate: sufficiently large to remove the finite-size artifacts, but not large enough to over-broaden the real features of the spectrum[5,6].

In our case we use Gaussian broadening, with the broadening parameter chosen as the parameter for which $\sigma_{\rm dc}$ is not changing or shows smallest change with broadening, a choice to which we refer as the optimal one. See Fig. S6. This prescription works also for finite and high frequencies, where the delta functions are denser and the spectra are smooth even with smaller broadening parameter. The used optimal broadening parameter is substantially smaller than the width of the Drude peak and we estimate the broadening uncertainty of $\rho_{\rm dc}$ within FTLM to be below 10%.

It is worth noting that that with increasing broadening the $\sigma_{\rm dc}$ drops monotonically. Since in all cases $\sigma_{\rm dc}$ in DMFT is lower, there must always be a certain broadening level that reproduces the DMFT result for $\sigma_{\rm dc}$, but not simultaneously $\sigma(\omega)$ at all frequencies. We have checked that the broadening level needed to reproduce $\sigma_{\rm dc}$ from DMFT is about 10 times the optimal one, and becomes comparable to the width of the Drude peak. This choice of broadening leads to severe modification in the shape of $\sigma(\omega)$, especially of the high-frequency peak which is otherwise well determined already by a fine binning of delta functions or with a tiny broadening. Therefore, we exclude such large broadening from consideration.

Finally, we note that for the calculation of $\Lambda(i\nu_n)$ from $\sigma(\omega)$ obtained by FTLM with Hilbert transform, Eq. (3) in the main text, no broadening is needed due to integration and that even if the broadened $\sigma(\omega)$ is used, $\Lambda(i\nu_n)$ change by the order of 10^{-5}, which is smaller than the symbol size in Fig. 3 (main text) and in Fig. S2 and is also below the CTINT noise level.

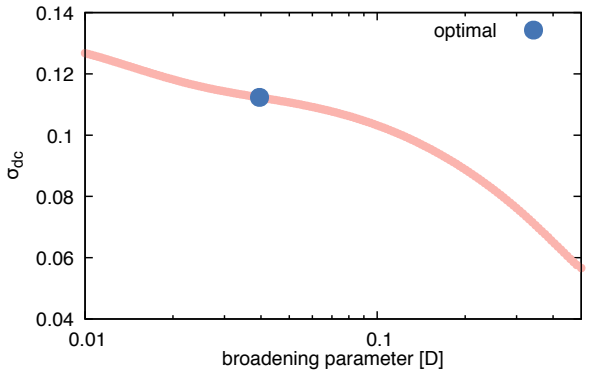

FIG. S6. Representative dependence of $\sigma_{\rm dc}$ from FTLM on the broadening parameter and the optimal parameter according to the minimal change of $\sigma_{\rm dc}$ with broadening. Data are for $p = 0.1$ and $T = 0.5D$.

[1] D. Bergeron, V. Hankevych, B. Kyung, and A.-M. S. Tremblay, Phys. Rev. B **84**, 085128 (2011).
[2] R. Levy, J. LeBlanc, and E. Gull, Computer Physics Communications **215**, 149 (2017).
[3] E. W. Huang, R. Sheppard, B. Moritz, and T. P. Devereaux, arXiv:1806.08346 (2018).
[4] E. Perepelitsky, A. Galatas, J. Mravlje, R. Žitko, E. Khatami, B. S. Shastry, and A. Georges, Phys. Rev. B **94**, 235115 (2016).
[5] J. Jaklič and P. Prelovšek, Adv. Phys. **49**, 1 (2000).
[6] J. Jaklič and P. Prelovšek, Phys. Rev. B **52**, 6903 (1995).